Smoke over haze: Comparative analysis of satellite, surface radiometer, and airborne in situ measurements of aerosol optical properties and radiative forcing over the eastern United States

Brian Vant-Hull,[1] Zhanqing Li,[1,2] Brett F. Taubman,[3] Robert Levy,[1,4]
Lackson Marufu,[1] Fu-Lung Chang,[5] Bruce G. Doddridge,[1] and Russell R. Dickerson[6]

[1]   In July 2002 Canadian forest fires produced a major smoke episode that blanketed the east coast of the United States. Properties of the smoke aerosol were measured in situ from aircraft, complementing operational Aerosol Robotic Network (AERONET), and Moderate Resolution Imaging Spectroradiometer (MODIS) remotely sensed aerosol retrievals. This study compares single scattering albedo and phase function derived from the in situ measurements and AERONET retrievals in order to evaluate their consistency for application to satellite retrievals of optical depth and radiative forcing. These optical properties were combined with MODIS reflectance observations to calculate optical depth. The use of AERONET optical properties yielded optical depths 2–16% lower than those directly measured by AERONET. The use of in situ–derived optical properties resulted in optical depths 22–43% higher than AERONET measurements. These higher optical depths are attributed primarily to the higher absorption measured in situ, which is roughly twice that retrieved by AERONET. The resulting satellite retrieved optical depths were in turn used to calculate integrated radiative forcing at both the surface and top of atmosphere. Comparisons to surface (Surface Radiation Budget Network (SURFRAD) and ISIS) and to satellite (Clouds and Earth Radiant Energy System CERES) broadband radiometer measurements demonstrate that the use of optical properties derived from the aircraft measurements provided a better broadband forcing estimate (21% error) than those derived from AERONET (33% error). Thus AERONET-derived optical properties produced better fits to optical depth measurements, while in situ properties resulted in better fits to forcing measurements. These apparent inconsistencies underline the significant challenges facing the aerosol community in achieving column closure between narrow and broadband measurements and calculations.

1.   Introduction

[2]   Aerosols produce significant radiative forcing at the surface, affecting both local weather patterns and global climate [*Ramanathan et al.*, 2001a; *Penner et al.*, 1992]. Absorbing aerosols have the additional effect of heating the atmosphere, which may impact cloud development both through local drop formation [*Ackerman et al.*, 1995; *Rosenfeld*, 1999] and stabilization of the atmospheric column [*Taubman et al.*, 2004; *Ackerman et al.*, 2000]. Smoke from biomass burning, which comprises nearly half of all absorbing aerosol throughout the world [*Ramanathan et al.*, 2001a], have particularly strong effects on surface and atmospheric radiation budgets [*Li*, 1998; *Li and Kou*, 1998].

[3]   Satellite retrievals are the most useful data set for climate studies because of their spatial and temporal coverage [*Kaufman et al.*, 2002]. These retrievals generally require prior knowledge of optical properties for the aerosol being retrieved [*King et al.*, 1999]. This poses a special difficulty for remote sensing of biomass burning aerosols whose optical properties vary widely depending on vegetation type, burning mode (smoldering or flaming), and age [*Kaufman et al.*, 1998; *Reid et al.*, 1999; *Wong and Li*, 2002]. One of the most important properties that characterize aerosol absorption is the single scattering albedo (ω_o).

[1]Department of Meteorology, University of Maryland, College Park, Maryland, USA.

[2]Also at Earth Systems Science Interdisciplinary Center, College Park, Maryland, USA.

[3]Department of Chemistry, University of Maryland, College Park, Maryland, USA.

[4]Also at Goddard Space Flight Center, Greenbelt, Maryland, USA.

[5]Earth Systems Science Interdisciplinary Center, College Park, Maryland, USA.

[6]Department of Meteorology and Department of Chemistry, University of Maryland, College Park, Maryland, USA.

The Smoke, Clouds, and Radiation-Brazil (SCAR-B) experiment [*Kaufman et al.*, 1998] in Brazil measured single scattering albedos as low as 0.6 (0.55 micron wavelength) in fresh smoke [*Reid et al.*, 1998b], increasing up to 0.91 as the smoke aged, associated with the growth of the particles as the liquid content increased. Measurements of Canadian smoke during the Boreal Ecosystem-Atmosphere Study (BOREAS) found ω_o to range from 0.70 for fresh smoke to 0.98 for aged smoke [*Miller and O'Neill*, 1997; *Li and Kou*, 1998]. Laboratory measurements of smoke emitted from pine needles from these trees show that ω_o for fresh smoke can range from 0.66 to 0.97 depending on whether the fire is in the flaming or smoldering phase [*Miller and O'Neill*, 1997]. Smoke may also evolve chemically during transport by mixing with other emissions [*Kreidenweis et al.*, 2001].

[4] This variability makes it impossible to evaluate the reliability of a single measurement or instrument, so field campaigns allow intercomparison between many instruments and measurement scenarios. In many previous field campaigns, a subset of aerosol optical properties (size distribution, phase function, optical depth) were retrieved from Sun photometers using algorithms that required fixed values for the remaining properties (complex index of refraction or single scattering albedo) [*Kaufman et al.*, 1998; *Russell et al.*, 1999b], while recent studies employ a more advanced and comprehensive algorithm proposed by *Dubovik et al.* [2000] for Sun photometer retrievals [*Dubovik et al.*, 2002]. Likewise, the absorption measurements using the particle soot absorption photometer (PSAP) instrument before 1999 could not take advantage of the *Bond et al.* [1999] calibration. In both the SCAR-B and Indian Ocean Experiment (INDOEX) experiments ω_o measured in situ by aircraft was 2 to 3 percent lower than that measured remotely by Sun photometer [*Dubovik et al.*, 2002; *Ramanathan et al.*, 2001b]. Though these differences are within instrumental error, the preponderance of lower values measured in situ versus Sun photometer suggests a true experimental difference. By contrast, much closer agreements were found between in situ and surface radiometer values of ω_o for aerosols dominated by biomass burning obtained during the Southern African Fire-Atmosphere Research Initiative (SAFARI) campaign [*Haywood et al.*, 2003; *Magi et al.*, 2003]. Other campaigns such as the Lindenberg Aerosol Characterization Experiment 1998 (LACE-98) [*Bundke et al.*, 2002] achieved consistency between measurement techniques by introducing a free parameter in the form of a variable liquid layer coating the carbonaceous core of aged smoke.

[5] Remote sensing and in situ measurements have complementary strengths and weaknesses. Passive remote sensing techniques retrieve column-averaged properties. Surface photometers such as those used in the Aerosol Robotic Network (AERONET) [*Holben et al.*, 1998] have the advantage of viewing the aerosol sample over a range of scattering angles, allowing the characterization of a complete suite of column-averaged aerosol optical properties [*Dubovik et al.*, 2000]. While remote sensing techniques do not perturb the measured aerosols, validity of the theoretical framework and assumptions dictates the quality of retrievals [*Remer et al.*, 1997; *Dubovik et al.*, 2000]. Satellite retrieval techniques must contend with a varying surface albedo and

a fixed viewing angle for any given location, both of which limit retrieval of a full set of optical properties. Usually one or several of the aerosol optical properties are fixed based on independent measurements (or assumption), and the remainder are derived from satellite measured reflectances [*Kaufman et al.*, 1990a; *Wang et al.*, 2003]. In situ observation techniques can resolve vertical profiles inaccessible to remote sensing. If properly calibrated [*Bond et al.*, 1999], they may be used to validate assumptions made in satellite retrievals. However, they may introduce additional errors from instrumental interaction with the measured aerosols [*Remer et al.*, 1997; *Bond et al.*, 1999]. Both in situ and Sun photometer measurements of aerosol optical properties have been incorporated into satellite retrieval algorithms [*Bundke et al.*, 2002; *Kaufman et al.*, 1998].
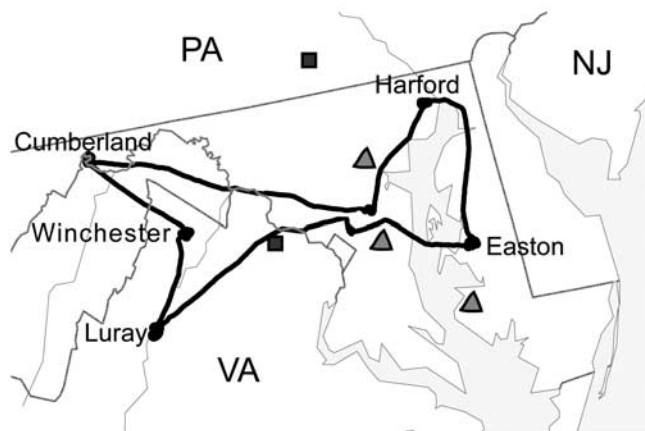
[6] This study examines the interplay between measurements of aerosol optical properties and satellite retrievals for a large smoke plume generated from forest fires in Canada in early July 2002 and advected along the eastern seaboard of the United States. During the fire episode, AERONET and aircraft in situ measurements were made on 8 July 2002 when a dense smoke plume swept across the Maryland/ Virginia area. It is the second in a series of studies based on aircraft measurements of optical properties, meteorological profiles, and trace gases. Our first study [*Taubman et al.*, 2004] demonstrated that radiative heating within the smoke layer may have maintained a subsidence inversion, thus slowing dispersal of the smoke. The current study continues with a synthesis of the aircraft measurements with surface radiometer and satellite observations of the same area and day in order to calculate radiative forcing across the region and to evaluate column closure among these different measurement systems of aerosol optical properties. Many of the above issues are addressed in this case study in which two independent measurements of aerosol optical properties are employed for satellite retrievals of aerosol optical depth and radiative forcing.

[7] The fire event, aircraft and ground observations are discussed in section 2. Determination of aerosol optical properties from various measurements is addressed in section 3. Comparisons between the two sets of aerosol optical properties are presented in section 4. When combined with the surface albedo and satellite measured top of atmosphere (TOA) reflectance for the same day, the radiative forcings are determined across the entire area for which the aircraft and AERONET measurements are assumed to be valid. The smoke radiative forcings at the TOA and surface are compared with those measured from space (CERES) and at the surface (surface radiation network of radiometers (SURFRAD); Integrated Surface Irradiance Study (ISIS)) for the two sets of optical properties. These are discussed in section 5. Section 6 presents a comprehensive uncertainty analysis of retrieved smoke optical depth and radiative forcing. A discussion of the possible reasons for discrepancies between the various measurements concludes the paper (section 7). The study is summarized in section 8.

2. Instrumentation and Data

2.1. In Situ Measurements

[8] The sampling platform, flight pattern, meteorology, instruments and calibrations used to acquire the in situ data

Figure 1. Flight path and locations of measurement spirals on 8 July 2002. The AERONET sites are indicated by triangles, surface broadband radiometer sites by squares.

for this study were described in detail in the work of *Taubman et al.* [2004], so only a brief description is given here. An instrumented light aircraft with aerosol and trace gas inlets engineered into the fuselage performed ascending or descending spiral flights between the surface and ∼3 km at each of the five locations shown in Figure 1. Owing to inlet impaction losses only submicron particle measurements are reported here. A Met One optical particle counter, particle soot absorption photometer (PSAP), and TSI integrating nephelometer were used to measure particle size distribution, absorption, and scattering, respectively.

[9] Two distinct aerosol layers were observed during the flights. Between the surface and 2 km, the optical properties were dominated by fossil fuel combustion aerosols common in the planetary boundary layer (PBL) of the region [*Novakov et al.*, 1997]. Larger, more absorbing smoke aerosol above 2 km was prevented from mixing down into the PBL by a morning subsidence inversion, which may have been maintained by absorptive heating of the smoke later in the day [*Taubman et al.*, 2004]. The natural decay in number density with height of the PBL aerosols and the lack of smoke vertical mixing meant that the layers could be treated as two independent modes. A selection of column averaged optical properties at each site is shown in Table 1. The area averaged optical properties measured by the aircraft appear in Table 2. All wavelength dependant values are listed for 550 nm only; the calculations necessary to transform the raw data into these values are described below. A weak smoke signal coupled with a coal burning power plant upwind of Cumberland invalidated the data at that site for the purposes of determining layer characteristics, and so is not included in the calculation of overall layer averages.

2.2. AERONET Measurements

[10] AERONET [*Holben et al.*, 1998] is an automated network of ground-based Sun photometers that measure aerosol optical thickness and sky radiance at six wavelengths (0.34, 0.38, 0.44, 0.67, 0.87 and 1.02 microns). From the sky radiance measurements aerosol size distributions and optical properties are derived operationally. Optical depth is calculated from attenuation of the solar direct beam, with uncertainties set by instrumental precision.

Uncertainty in all other optical properties depends on the reliability of the plane parallel assumption for a large set of measurements at different angles as well as the numerical algorithmic precision.

[11] There are three AERONET sites in the region loosely defined by the aircraft flights. The Goddard Space Flight Center (GSFC) site is located at the edge of the greater Washington, DC, metropolitan area. Quality assured retrievals of optical depth fluctuated between 1.3 and 2.2 throughout the day of the aircraft measurements, indicating the influence of smoke for the entire day. Optical depths as high as ∼7 could be inferred for later in the day at this and other sites, though low radiances degraded the quality of the retrievals and so these higher values were not publicly distributed [*Eck et al.*, 2003]. The Smithsonian Environmental Research Center (SERC) site is on a sparsely inhabited peninsula protruding into the Chesapeake Bay, and also showed high optical depths throughout the day but with smaller variability (between 1.8 and 2.2). The Maryland Science Center (MDSC) site is located in downtown Baltimore, MD, next to the harbor and showed generally lower optical depths between 1.3 and 1.8.

[12] Throughout the day the smoke layer was optically several times thicker than the underlying PBL aerosol (average optical depth of 0.34 as measured by the aircraft). By consequence AERONET retrievals should strongly reflect the smoke properties, though the PBL aerosol is closer to the instrument and its influence cannot be ignored. Table 2 compares aerosol properties retrieved from the AERONET [*Dubovik et al.*, 2000] at the GSFC site for the day of the flight against those obtained from the aircraft in situ measurements. They represent fine mode aerosol, as the almucantar retrievals indicate that the coarse mode comprised only 3% of the total optical depth at 0.55 μm. Two values of the AERONET asymmetry parameter are

Table 1. Average Single Scattering Albedo and Scattering Ångström Exponents for Each Site at 0.55 Micron Wavelength[a]

	ω_o 550 nm	$\alpha_{450/550}$	$\alpha_{550/700}$
	Luray		
Smoke	0.91 ± 0.02	0.57 ± 0.18	1.04 ± 0.11
PBL	0.95 ± 0.01	1.84 ± 0.42	1.99 ± 0.34
	Winchester		
Smoke	0.94 ± 0.01	0.60 ± 0.44	1.05 ± 0.22
PBL	0.95 ± 0.01	1.90 ± 0.34	2.06 ± 0.30
	Cumberland		
Smoke	0.86 ± 0.03	1.17 ± 0.64	1.29 ± 0.30
PBL	0.94 ± 0.01	1.85 ± 0.26	2.05 ± 0.21
	Harford		
Smoke	0.93 ± 0.01	0.87 ± 0.10	1.26 ± 0.09
PBL	0.94 ± 0.01	1.45 ± 0.33	1.70 ± 0.29
	Easton		
Smoke	0.93 ± 0.01	0.71 ± 0.10	1.18 ± 0.09
PBL	0.96 ± 0.01	1.83 ± 0.19	2.03 ± 0.16
	Average		
Smoke	0.93 ± 0.02	0.69 ± 0.11	1.14 ± 0.09
PBL	0.95 ± 0.01	1.76 ± 0.31	1.96 ± 0.30

[a]Uncertainties are given as one standard deviation. The area averages are weighted by the optical depth of each site, with Cumberland excluded.

Table 2. Averaged Aerosol Parameters for the Three Optical Models[a]

	Effective Radius, r_e, μm	Variance δ, ln r	Refractive Index, n + ik	Single Scattering Albedo, ω_o	Asymmetry Parameter, g
AERONET GSFC	0.15	0.61	1.56 + .0067i	0.964 ± .03	0.65/0.62
Aircraft smoke	0.22	0.46	1.58 + 0.015i	0.930 ± .02	0.66 ± .04
Aircraft PBL	0.08	0.86	1.43 + 0.006i	0.949 ± .02	0.62 ± .04

[a]Wavelength-dependent quantities are given for 0.55 microns. AERONET values represent a total column average, interpolated to 0.55 μm, with algorithm uncertainties quoted for ω_o. Instrumental (but not statistical) uncertainties are quoted for the aircraft values of ω_o. The uncertainties for g are a composite of uncertainties in the instruments and the assumption of index of refraction (see section 6).

listed: g = 0.65 is the listed value, while g = 0.62 comes from applying Mie theory calculations to the retrieved index of refraction and size distribution [*Mishchenko et al.*, 2002]. When optical depth was retrieved by satellite using phase functions calculated from Mie theory (corresponding to the lower value of the asymmetry parameter), the results were nearly identical to optical depth retrievals using the higher listed value of the asymmetry parameter in the Henyey-Greenstein phase function. For consistency the Mie theory calculations are used throughout this study. The MDSC values of ω_o and asymmetry parameter were slightly higher than the GSFC values, possibly due to the location in a highly urbanized area. These values, therefore, were not considered as representative for the entire plume as those from GSFC and were not used in subsequent calculations. Only optical depth was retrieved by the SERC site, and in the clear days that immediately followed the smoke event, low optical depths prevented retrieval of other aerosol optical properties at any of the sites.

3. Determination of Optical Properties and Optical Depth

3.1. Size Distributions

[13] The Met One optical particle counter measured aerosols in six size bins from 0.3 to 1.0 micrometer optical diameter. Impaction losses adversely biased the counts of higher diameters and skew the size distribution extrapolated from this narrow range, while the optically significant aerosol population below 0.3 micrometer diameter is not represented. A monomodal size distribution was therefore inferred by matching the scattering Ångström exponents measured by the nephelometer for the wavelength pairs (450/550 nm) and (550/700 nm) to those calculated by Mie theory for adjustable lognormal distributions [*Mishchenko et al.*, 2002].

[14] The real part of the index of refraction retrieved by AERONET was assumed to be a weighted average of the PBL climatology average of 1.43 [*Remer et al.*, 1997; *Dubovik et al.*, 2002] and that of smoke. An AERONET value of n = 1.56 thus implies a smoke value of n = 1.58 under the assumption of smoke being approximately 5 times thicker than the underlying aerosol as measured by the aircraft. Though higher than the average this value falls within the range of other measurements for smoke from this region [*Fiebig et al.*, 2002]. For moderate absorption the scattering exhibits no significant dependence on the imaginary part of the index of refraction, which is set to a nominal value for this part of the calculation.

[15] Figure 2a shows the lognormal curves of the size distributions for the smoke and PBL layers derived from the Ångström exponents, together with data points from the Met One measured size distributions as a consistency check. The AERONET retrieval is given for comparison. Though the lognormal curve for the AERONET distribution was based directly on statistics from the data, the volume weighted curve does not appear to fit the data well. Figure 2b re-plots the AERONET data in the more radiatively significant area weighted form that accentuates the lower wing of the distribution. A bimodal distribution is now clearly visible, with the lognormal curve expected to serve as an optically equivalent average distribution [*Tanre et al.*, 1996]. Table 2 presents the volume-weighted radius and variance for the lognormal curves fitted to the AERONET retrieval, with the PBL aerosol and smoke values derived from Ångström exponents. As expected for a column average, the smoke and PBL values bracket those of AERONET.
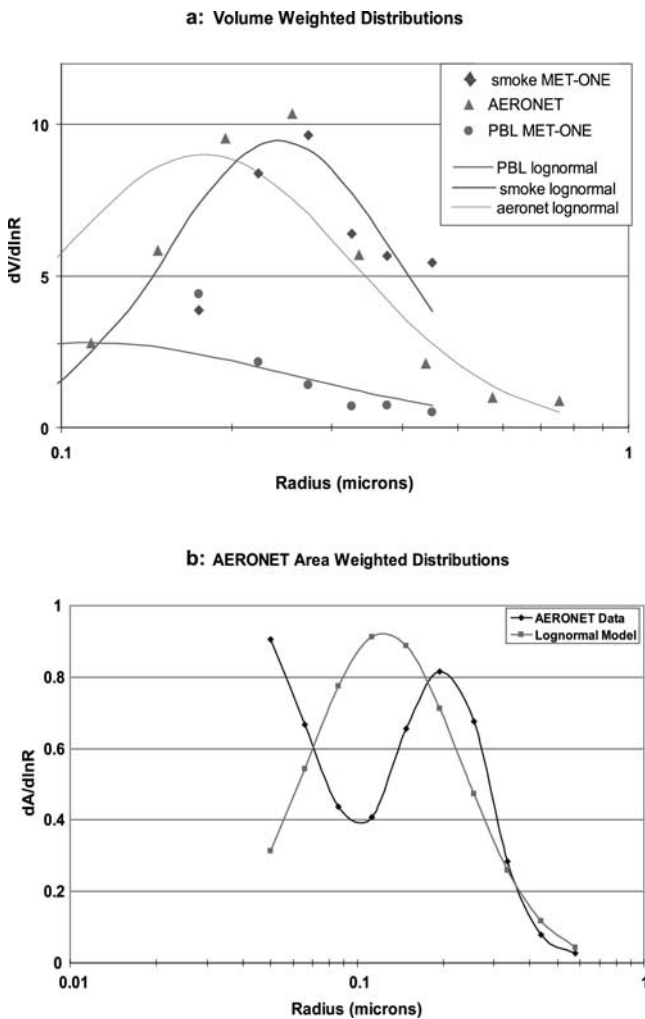
[16] In a similar manner to the real index of refraction, the column averaged volume weighted radius retrieved from AERONET was 0.18 μm (corresponding to the effective radius of 0.15 μm listed in Table 2), with a climatological PBL average of 0.16 μm for an optical depth of 1.5. Since these two values are close together, the effective radius of the predominant smoke component will be very close to the column average. The column averaged size distribution retrieved by AERONET, therefore, was used to represent pure smoke.

3.2. Optical Properties

[17] In situ values of scattering and absorption cross sections were used to calculate the single scattering albedo for the aircraft data. The absorption measurement at 565 nm was extrapolated to 550 nm to match the central scattering measurement. Assuming all the absorption is due to black carbon, the variation of the imaginary part of the index of refraction with wavelength is very weak over this interval [*Chang and Charalampopoulos*, 1990] and the absorption is expected to follow a $1/\lambda$ dependence [*Bergstrom et al.*, 2002; *Bohren and Huffman*, 1983].

[18] The column averaged AERONET value of ω_o interpolated to 550 nm is about 0.964. At GSFC the climatological value (1998–2001) of ω_o is 0.98 ± .02 [*Dubovik et al.*, 2002]. Assuming the ω_o retrieval represents a weighted average of PBL aerosol with approximately 5 times as much smoke aerosol, the smoke ω_o would be about 0.962. Since this value is not a significant departure from the original AERONET value, the column averaged ω_o was used to represent smoke.

[19] Mie theory calculations of scattering phase functions were based on the size distributions and index of refraction [*Mishchenko et al.*, 2002]. Eight terms in the Legendre

a: Volume Weighted Distributions

b: AERONET Area Weighted Distributions

Figure 2. (a) Population per cubic centimeter: Met One smoke data points (diamonds), Met One PBL aerosol data points (circles), and AERONET retrievals (triangles). The solid lines are lognormal fits to scattering Ångström exponents from in situ data. The dotted line is based on statistics from the AERONET retrieval. The amplitude of each lognormal curve is adjusted to best fit for all points. (b) Area weighted distribution for the AERONET retrieval (blue) and the lognormal curve based on statistics from the retrieval. Vertical units are arbitrary. See color version of this figure at back of this issue.

polynomial expansion of this phase function were used for all retrievals described below.

3.3. Optical Depth Estimated From Satellite

[20] The satellite retrievals described in this section assume that aerosol ω_o and phase function measured at one location are valid throughout the area shown in Figure 1. The in situ measurements at the four locations and the three AERONET sites all showed variations from the mean values that were within the instrumental and statistical uncertainties of the respective instruments and data sets (see Tables 1 and 2, the sensitivity section below, and *Dubovik et al.* [2000]). It is therefore consistent to assume average values for these properties within the area defined

by the flight locations. On the basis of the size of the meteorological system in which the measurements were made, the study area was extended across several degrees of latitude and longitude in order to include all three AERONET sites and the SURFRAD site depicted in Figure 1.
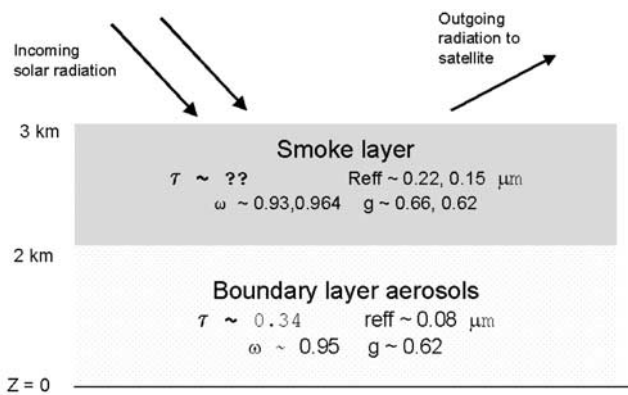
[21] The satellite TOA radiances were measured in band 4 (550 nm) of the MODIS instrument at 5 km resolution, using the Terra overpass from 1540 to 1545 GMT. This band was chosen because it was closest to the in situ absorption measurement at 565 nm while corresponding directly to one of the scattering wavelengths measured. It is also in the middle of the range of wavelengths retrieved by AERONET, so properties such as index of refraction and single scattering albedo may be easily interpolated.

[22] The Santa Barbara Discrete-Ordinate Atmospheric Radiative Transfer (SBDART) code was used for all radiative calculations [*Ricchiazzi et al.*, 1998], using the LOW-TRAN-7 solar spectrum and sixteen streams. Tests have been conducted in which the radiance outputs of the satellite algorithm for retrieved optical depths were compared to an adding-doubling radiation transfer code written in-house and extensively validated by *Chang et al.* [2000]. The comparisons agree to within a few W/m^2/steradian. Atmospheric inputs included average aircraft measurements of temperature, ozone, and water vapor up to 3 km, with the standard midlatitude summer atmosphere above 3 km.

[23] The surface albedo used was the MODIS land team level 3 eight-day reflectance product [*Vermote and Vermeulen*, 1999]. This product uses a composite of cloud-free scenes to calculate surface reflectance at each wavelength, with an aerosol correction technique similar to that used by the MODIS atmosphere team aerosol product [*Kaufman et al.*, 1998]. The period chosen was roughly 2–3 weeks after the smoke event, in which the average aerosol optical depth was typically 0.2 or less, thus reducing correction uncertainties. Nadir view scenes are preferentially selected for this product, and the time of the satellite overpass used in this study was close to noon, reducing the need for angular corrections.

[24] A two-layer aerosol as depicted in Figure 3 was assumed: the PBL aerosol in the layer from the surface to 2 km, with the smoke added to the layer from 2 to 3 km. The PBL aerosol was set to the average optical depth of 0.34 ± 0.1 as measured by the aircraft, with a ω_o of $0.95 \pm .01$ and an asymmetry parameter of 0.62. The uncertainty in optical depth is due to the spatial variability between measurement spirals. The smoke optical properties were derived either from the average aircraft values ($\omega_o = 0.93$ and g = 0.66) or AERONET retrievals ($\omega_o = 0.963$ and g = 0.62). To perform a satellite retrieval of optical depth, aerosol in the PBL layer was assumed to be spatially invariant while the quantity of smoke was adjusted until the calculated and measured radiances at TOA matched.

[25] Visible MODIS imagery for the Terra satellite at 1540 GMT shows how the addition of smoke brightens the scene from dark to gray (Figure 4a). It is not easy to distinguish between thick smoke and cloud using visible wavelengths. As shown in Figure 4b the MODIS operational cloud screen, using a combination of visible and brightness temperature thresholds, misidentified smoke as clouds since training sets typically do not include thick

Figure 3. Two-layer model in which the smoke layer optical depth must be adjusted until the outgoing radiance matches that observed by satellite. The smoke parameters come either from the aircraft in situ measurements or from AERONET.
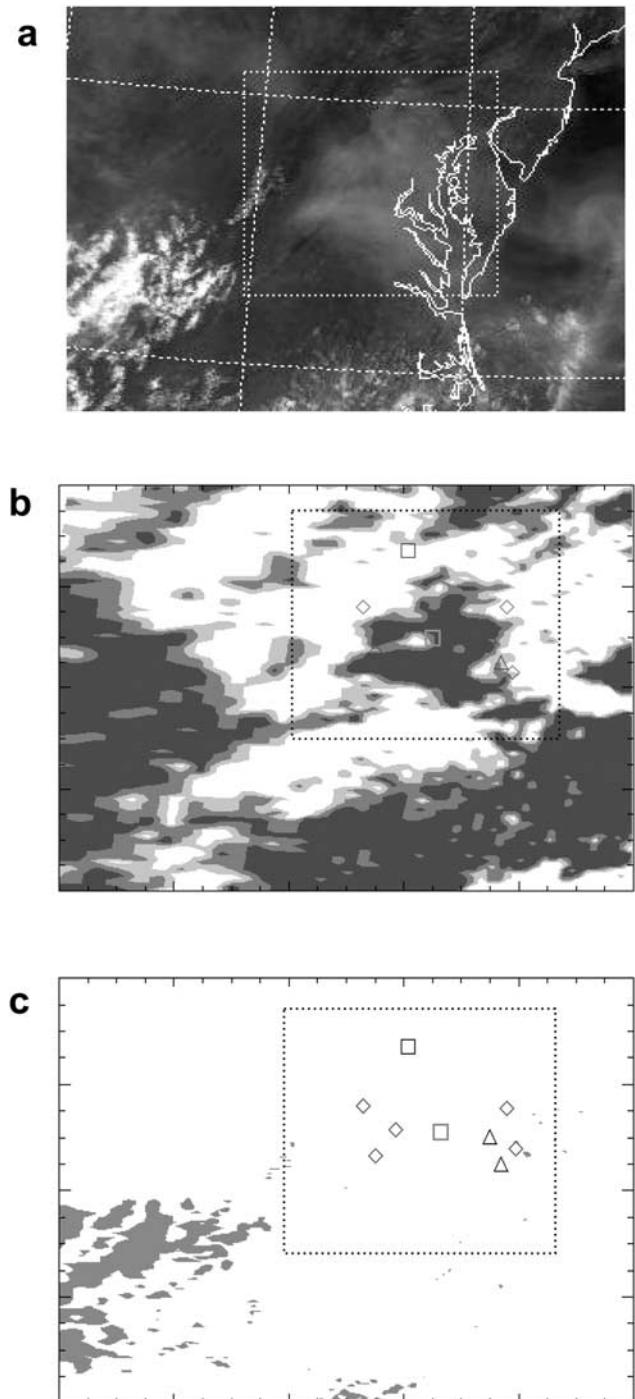
smoke plumes. With cloud droplets typically a few microns in radius while smoke particles fall in the submicron range, reflectivity in the near IR wavelengths may be used to distinguish between the two [*Kaufman et al.*, 1990b]. A cloud screen based on near-infrared (NIR) thresholds indicates that the area under analysis is almost entirely cloud-free (Figure 4c).

4. Comparisons of Satellite Optical Depth Retrievals

[26] A comparison of the two sets of aerosol optical properties is summarized in Table 2. Although the size distribution parameters for smoke and PBL aerosol bracket those of AERONET, the single scattering albedo for AERONET is higher than either in situ measurement. Sensitivity tests in a later section demonstrate that this difference is the primary factor in disparities between the optical depth retrievals.

[27] The AERONET observed optical depth at each of the three sites within the region of interest was compared to the satellite retrieved optical depth calculated from two primary optical models: AERONET column average, or in situ layered structure as measured by aircraft. Two mixed models employ the same PBL layer, but use combinations of aircraft and AERONET ω_o and phase functions in the smoke layer (Table 3).

[28] For purposes of comparison, AERONET optical depth measurements at wavelengths of 440 and 670 nm were interpolated logarithmically to 550 nm, and also interpolated linearly in time to match the satellite overpass. The stated algorithm uncertainty for the AERONET observations is ±0.02 [*Holben et al.*, 1998] with the interpolations also adding estimated uncertainties up to ±.02. The optical depths measured by AERONET and calculated by satellite data for the four models are shown in Table 3. The four pixels that fall within a 0.1° box centered on each sensor were averaged so that data within a radius of about 7 km were included; the uncertainties shown are the sample standard deviations only. One of the points in the SERC

Figure 4. Examination of cloud screening algorithms to distinguish smoke from cloud for 1540 Z, 8 July 2002. In the cloud mask images, clouds are denoted by gray; clear by white. The dotted line boxes indicate the approximate region of study. Geometric symbols represent measurement locations as described in Figure 1. The NIR threshold screening indicates that smoke, not cloud, covers the study area. (a) MODIS visible imagery at time of overpass. (b) MODIS cloud mask product. (c) Smoke/cloud screen based on NIR threshold.

Table 3. Comparison of Aerosol Optical Depth Retrievals[a]

Single Scattering Albedo	Scattering Phase Functions	GSFC (4 Pixels)	SERC (3 Pixels)	MDSC (4 Pixels)
In situ + PBL	**in situ + PBL**	**2.25 ± .10**	**2.18 ± .26**	**1.92 ± .08**
AERONET + PBL	in situ + PBL	1.71 ± .07	1.67 ± .21	1.46 ± .06
AERONET+ PBL	AERONET+ PBL	1.55 ± .06	1.51 ± .19	1.33 ± .05
Pure AERONET	**pure AERONET**	**1.54 ± .06**	**1.50 ± .19**	**1.31 ± .05**
AERONET observations		*1.68 ± .04*	*1.79 ± .03*	*1.34 ± .04*
MODIS standard smoke model		*2.02 ± .45*	*1.93 ± .44*	*- - -*
MODIS operational eastern U.S. model		*1.69 ± .39*	*1.64 ± .38*	*- - -*

[a]The first three rows show the satellite retrieved optical depth added to the assumed optical depth of the PBL aerosol, and the fourth row is a satellite retrieval of the total aerosol column based on AERONET-derived properties. The source of the optical parameters used as inputs are listed on the left. Uncertainties denote the variation in retrieved values from surrounding pixels only and do not reflect instrument or algorithm errors. The fifth row lists the optical depths observed by AERONET interpolated to the time of the satellite overpass, with instrumental and interpolation uncertainties included. The last two rows list the MODIS retrieval using the smoke model used in the western United States and the operational retrieval, with algorithmic uncertainties included. Boldface values refer to satellite retrievals using a single type of measurement, while italic values refer to a direct measurement itself.

set was over the bay with spuriously high surface reflectance, and so was rejected.

[29] MODIS aerosol retrievals are included for comparison due to general interest in this operational data set. Values of optical depth were generated for both the smoke model used in the western United States and the operational retrieval for the eastern United States with cloud screening turned off. The operational values of $\omega_o = 0.96$ and $g = 0.66$ are closer to the AERONET retrievals than any of the other models, yielding a value of optical depth very close to that directly observed by AERONET.

[30] Satellite retrievals using the aircraft and AERONET optical properties produced the highest and lowest optical depths, respectively, with the mixed models exploring the sensitivity of satellite retrievals to absorption (represented by ω_o) and size distribution (represented by scattering phase functions). The largest change is due to variations in ω_o: the roughly 30% increase in optical depth is disproportionate to the 3.5% decrease in scattering per photon interaction. For large optical depths multiple scattering assumes a dominant role [*Bohren*, 1987], and with multiple chances for each photon to be absorbed the decrease in reflected light is a nonlinear function of the single scattering albedo [*Wong and Li*, 2002]. When aircraft scattering phase functions are changed to those from AERONET the retrieved optical depth decreases by roughly 10%, as expected for increased backscattering due to smaller particles. Use of the PBL aerosol layer with an AERONET smoke layer produces an optical depth almost identical to the pure AERONET aerosol: the combination of lower ω_o with smaller particles at the bottom of the plume produces nearly the same TOA reflectance.

[31] The effect of a thick absorbing aerosol is apparent in the regional distribution of satellite retrieved optical depth (Figure 5). For the 1540 GMT Terra satellite overpass the two primary models are shown, with the MODIS operational retrieval exhibited for comparison with the cloud screening turned off (Figure 5d) [*Kaufman and Fraser*, 1997]. Ratios between the optical depths of the two models show that the model disparity increases with optical depth (Figure 5c).

[32] The gray areas in the upper left of Figure 5 indicate areas where the calculated amount of reflectance from the assumed PBL aerosol optical depth of 0.34 was larger than the satellite observation. They correspond to mountainous regions of clearer air. The gray areas that lie in a line

between the two AERONET sites correspond to parts of the Chesapeake Bay where the surface reflectance product produced spuriously high reflectances, and so these points must also be rejected. Other scattered gray areas are the result of the cloud-screening algorithm.

[33] The comparison demonstrates the high sensitivity of satellite-based retrieval of aerosol optical depth to the aerosol optical properties. The retrievals using AERONET optical properties are the lowest, while those using in situ measurements are the highest. As shown in Figure 5c for thick plumes it is not uncommon to see ratios of 1.5 or more. We may thus argue that the aerosol optical depth retrieved by satellite is subject to considerable uncertainty linked to the measured optical properties used as inputs, especially for thick layers of absorbing aerosol.
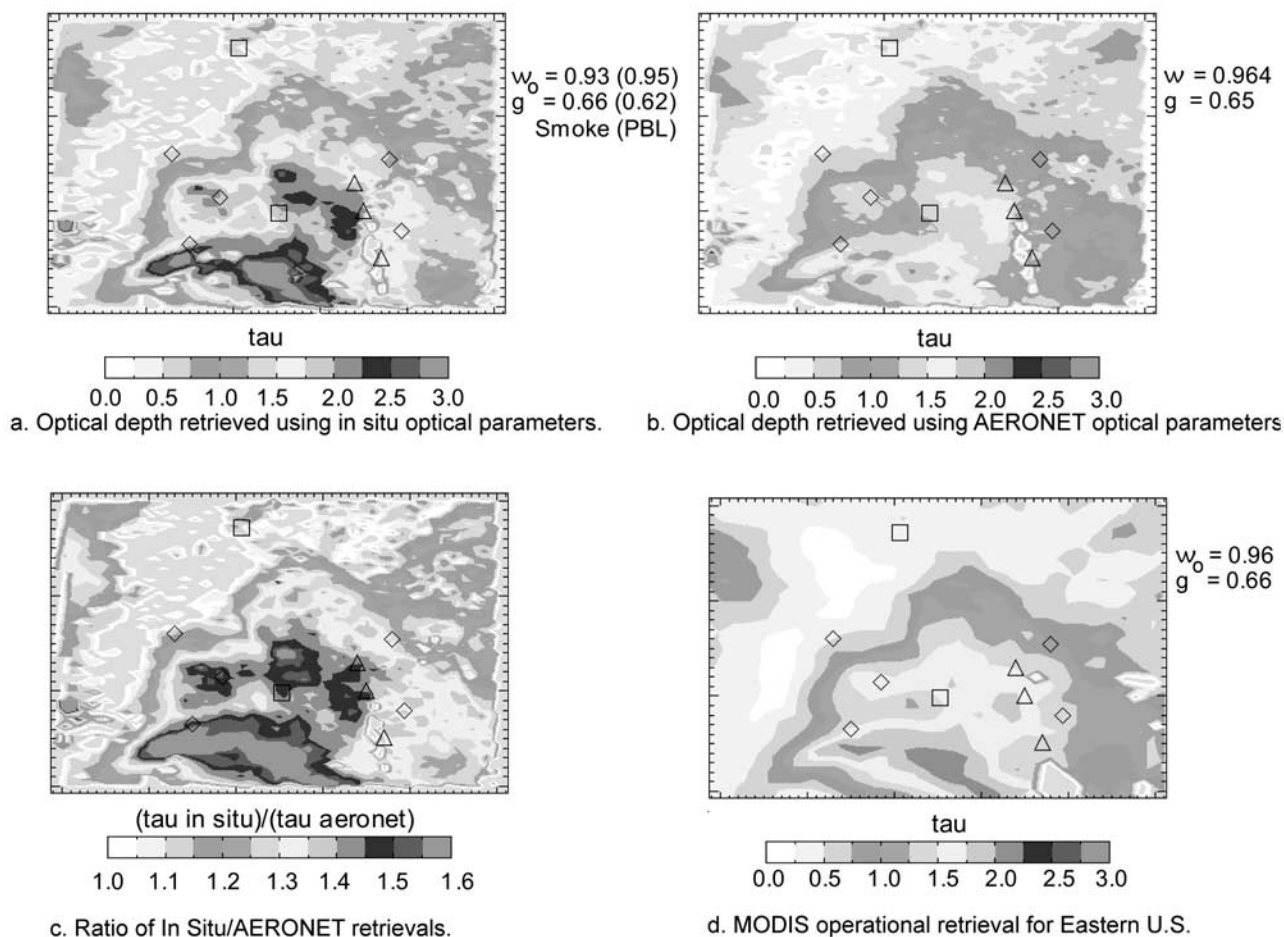
5. Forcings

[34] One of the most significant impacts of a thick smoke plume is its radiative forcing at the surface and in the atmosphere [*Li and Kou*, 1998; *Hobbs et al.*, 1997]. Satellite retrievals of optical depth together with aircraft and/or ground based measurements of aerosol optical properties allow the forcings to be calculated at any point. As an evaluation of column closure these calculations will be compared against broadband fluxes at the surface as measured by the Pennsylvania SURFRAD and the Virginia ISIS sites, as well as estimates of TOA fluxes obtained from the CERES satellite radiometer.

5.1. Extrapolation of Optical Properties

[35] To compute broadband radiative fluxes the single value of absorption measured at 565 nm and the three measurements of scattering at 450, 550 and 700 nm must be extrapolated across the solar spectrum from 0.3 to 3 micrometers. The size distributions inferred by matching Mie calculations to the Ångström exponents at these wavelengths may be used to calculated optical properties at any other wavelength [*Mishchenko et al.*, 2002], but only if the real and imaginary parts of the index of refraction are known across the spectrum.

[36] The most likely composition of aged smoke is a carbonaceous core with a sheath of a water/sulphate mixture [*Fiebig et al.*, 2002; *Remer et al.*, 1998]. The core would be composed of black carbon (soot) and other organic compounds [*Conny and Slater*, 2002]. With the exact composi-

Figure 5. Comparison of optical depth retrievals via satellite. For symbol definition, see Figure 1. The color scale ranges from 1 to 3. (a) Optical depth retrieved using in situ optical parameters. (b) Optical depth retrieved using AERONET optical parameters. (c) Ratio of in situ/AERONET retrievals. (d) MODIS operational retrieval for the eastern United States. See color version of this figure at back of this issue.
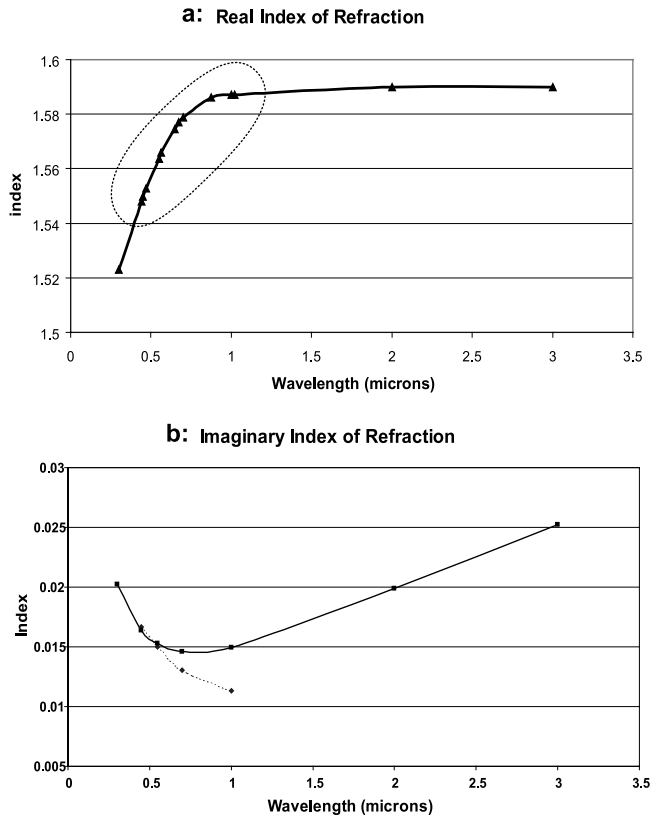
tion unknown, the real part of the index of refraction was based on extrapolation of AERONET measurements, as shown in Figure 6a. For comparison, *Torres et al.* [2002] assumed a constant real index of refraction of 1.55 throughout the UV and visible for carbonaceous aerosols based on a number of measurements. Our values are slightly lower in the UV (n = 1.52 to 1.54) and slightly higher in the visible and NIR (n = 1.55 to 1.59), with a trend that resembles the *Chang and Charalampopoulos* [1990] measurements for black carbon. The imaginary part is commonly assumed to be due entirely to black carbon content [*Bergstrom et al.*, 2002; *Ramanathan et al.*, 2001a; *Fiebig et al.*, 2002]. Since the measured properties of soot vary widely with composition [*Bergstrom et al.*, 2002; *Russell et al.*, 1999b], the most applicable carbon absorption measurements must be selected to match observations in this area. Similar work was done during the Tropospheric Aerosol Radiative Forcing Observation Experiment (TARFOX) [*Bergstrom et al.*, 2002; *Russell et al.*, 1999a], in which smoke was assumed to be mixed with aerosols from the same general area of the current study. It was concluded that measurements of the refractive index of soot made by *Chang and Charalampopoulos* [1990] provide the best fit to observed

data, and so the same data set will be used here. For the present study the imaginary index of refraction at 550 nm was adjusted until the calculated ω_o matched the in situ measurements, and the proportionality between this value and the soot data was used to calculate the imaginary refraction index at all other wavelengths (Figure 6b). This is equivalent to adjusting the composition of black carbon as done in TARFOX.

5.2. Forcing Calculations and Comparison

[37] With scattering and absorption cross sections at every wavelength calculated by Mie theory, aerosol optical depth measured at one wavelength was used to determine the optical depth at all other wavelengths by proportionalities, and the spectrally integrated radiative forcing calculated as a result. This technique was applied to the satellite-derived maps of optical depth at 0.55 μm described above. The MODIS land team reflectances were used up to 2.1 microns (as described in the algorithm theoretical basis document listed above) with the CERES mixed vegetation albedos used for higher wavelengths (from code available at the surface and radiation budget working group Web page: http://snowdog.larc.nasa.gov/pub/surf/pages/explan.html).

Figure 6. Real and imaginary parts of the index of refraction. (a) The real part, extrapolated from AERONET, with the circled region showing the original retrieval. (b) The imaginary part, proportional to that measured for black carbon, with the AERONET retrievals shown as a dotted line, both adjusted to provide the measured ω_o at 550 nm.

Surface and TOA maps of integrated fluxes or forcing allow comparison to observations.

[38] Table 4 shows a comparison of spectrally integrated surface forcing measurements (clear sky flux minus smoky sky flux) taken by SURFRAD and ISIS instruments to calculations of the four optical models used in this paper. All measurements and calculations correspond to the time of the satellite overpass, with temporal interpolation of the data as needed. The low optical depth at the SURFRAD site means the column is dominated by the PBL aerosol, while the ISIS site is dominated by smoke. In both cases the aircraft in situ model performed best: calculations were

about 10% below measurements when dominated by PBL aerosol, and about 20% high when dominated by smoke. Forcings calculated for the pure AERONET model was half the measured value when dominated by PBL aerosol, 2/3 when dominated by smoke.
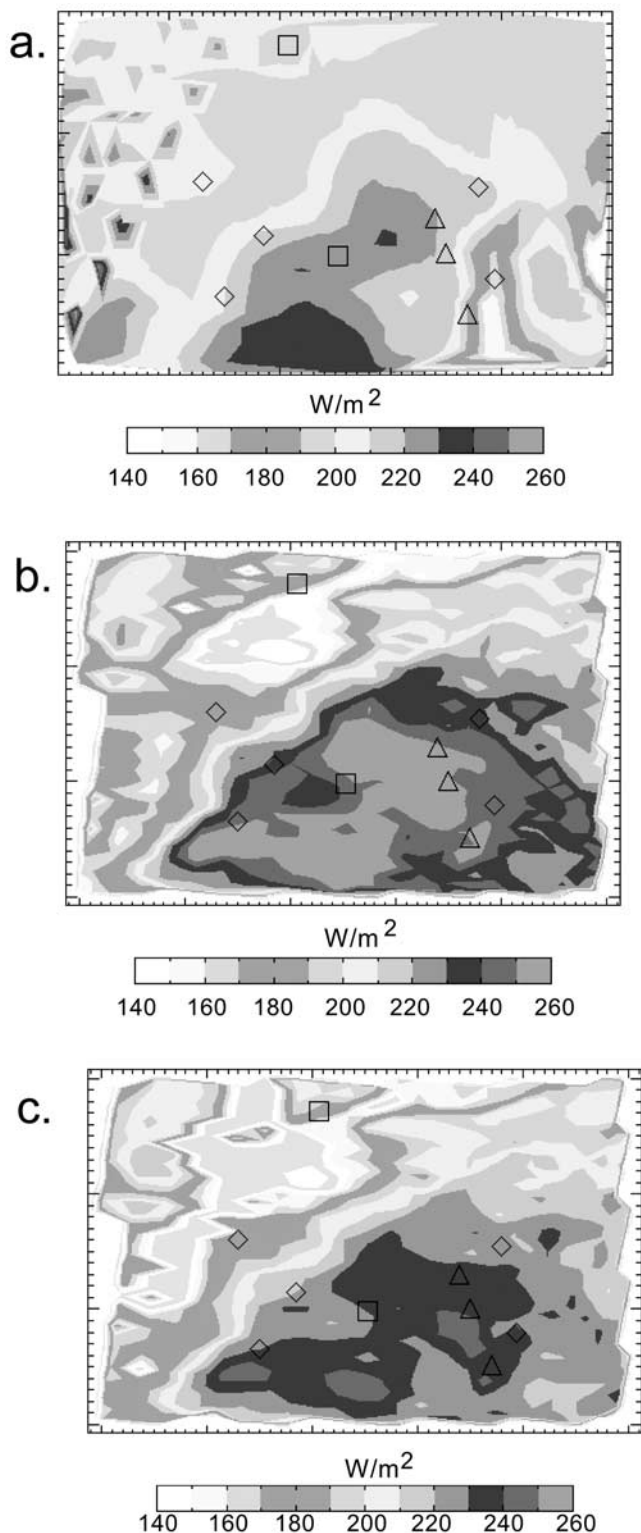
[39] It is unlikely that the low calculated values for the AERONET optical properties are due to the use of fine-mode retrievals alone: although the proportion of optical depth due to coarse mode increases with wavelength, the almucantar retrievals indicate the coarse mode optical depth at 1.02 microns was less than 10% of the total optical depth. Even if the coarse mode comes to dominate the forcing in the longer wavelengths the solar spectrum contains insufficient energy in this region to contribute significantly to the total forcing. The larger surface forcing calculated for the aircraft model is due in large part to the retrieval of larger optical depths, which in turn is due primarily to larger absorption measurements. Note that the size distribution affects the spectral variations of aerosol optical depth and single scattering albedo. At the SURFRAD site as the model changed from AERONET + PBL to pure AERONET, the decrease in forcing was largely due to substituting the significantly narrower AERONET size distribution for the dominant PBL distribution. Broadband forcing is the integral of spectral forcing at each wavelength. A narrow size distribution produces a narrow scattering spectrum. Broader size distributions thus produce a larger broadband forcing as the scattering spectrum is integrated across the wavelength domain.

[40] The CERES instrument, mounted on the same satellite platform as the MODIS instrument used to retrieve optical depth, provides broadband radiation measurements that can be used to estimate TOA forcing. The product used was the Earth Radiation Budget Experiment (ERBE)–like inversion of radiance to instantaneous TOA flux (ES-08) [*Green and Robbins*, 1997]. In this product the measured radiances are converted to fluxes using anisotropy functions based on inferred surface type. This data set must then be considered to be a retrieval rather than a measurement of broadband flux. In Figure 7 the TOA flux retrieved by CERES is compared to that calculated using the aircraft and AERONET aerosol optical models based on the retrieved optical depths. The fluxes calculated by both models are higher than those retrieved by CERES, though the aircraft model is significantly closer to the CERES data. Since the retrieved optical depth using the AERONET model is lower than that using the aircraft model, the larger forcing is due entirely to the aerosol optical properties: smaller, less

Table 4. Broadband Surface Aerosol Radiative Forcing at the Two Radiometer Sites[a]

Single Scattering Albedo	Scattering Phase Functions	SURFRAD 1541 Z		ISIS 1541 Z	
		Tau	Forcing, W/m^2	Tau	Forcing, W/m^2
In situ + PBL	**in situ + PBL**	**0.57 ± .12**	**−102 ± 19**	**1.93 ± .09**	**−297 ± 11**
AERONET + PBL	in situ + PBL	0.53 ± .09	−87 ± 12	1.47 ± .04	−193 ± 4
AERONET + PBL	AERONET + PBL	0.51 ± .08	−88 ± 12	1.33 ± .03	−188 ± 3
Pure AERONET	**pure AERONET**	**0.45 ± .12**	**−58 ± 17**	**1.32 ± .03**	**−166 ± 3**
Measured forcing			*−113 ± 11*		*−246 ± 8*

    [a]The top four rows are calculations based on satellite retrievals of optical depth, and the bottom row shows the actual measurements. Uncertainties indicate spatial variation between pixels surrounding the site for the satellite retrievals and temporal interpolation uncertainty for radiometers. Boldface values refer to satellite retrievals using a single type of measurement, while italic values refer to a direct measurement itself.

Figure 7. Comparisons of flux measurements to calculations from the two primary optical models. For symbol definitions, see Figure 1. The gray areas are undefined data. (a) TOA flux retrieved by CERES. (b) TOA flux calculated from the AERONET model. (c) TOA flux calculated from the in situ model. See color version of this figure at back of this issue.

absorbing particles with a broader distribution produce a larger backscatter signature than the smoke particles measured by the aircraft. This is similar to the SURFRAD case in which the predominance of the smaller PBL aerosol with a broad distribution produced larger surface forcing than the AERONET model aerosol.

[41] The presence of aerosol darkens the surface, increases the reflected flux at TOA, and causes atmospheric heating by absorption. Maps of surface forcing, TOA forcing, and absorption for the two primary models appear in Figure 8. Given that the flux measurements at the surface and TOA both came closer to agreement with the aircraft optical model, the calculated forcing based on the aircraft model may be closer to reality.

6. Uncertainty Analysis

6.1. Uncertainty in Determining Smoke Optical Depth

6.1.1. Absorption and Single Scattering Albedo

[42] For a fixed TOA reflectance, satellite-derived optical depth varies rapidly with single scattering albedo as shown in Figure 9. It is seen that an increase in ω_o results in a decrease in optical depth at a rate that grows with optical depth. There is no simple relation that captures this behavior perfectly; a rough approximation for the range of optical depths in Figure 9 is achieved by the relation

$$\Delta\tau \approx -\left(5\tau^{5/2}\right)\Delta\omega_o. \qquad (1)$$
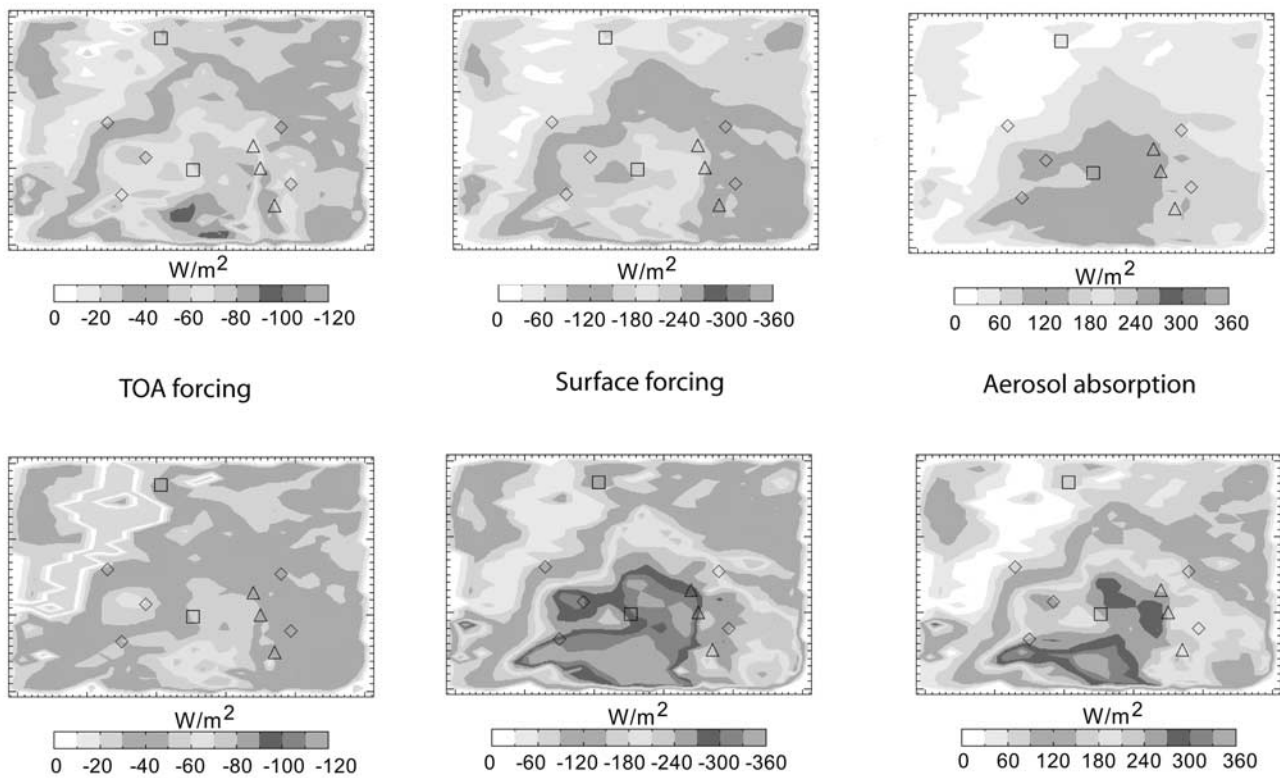
So for the typical optical depth $\tau = 2$, an increase in the single scattering albedo of 0.01 results in a decrease in optical depth of ~0.28 or 14%. When the AERONET retrieval of $\omega_o = 0.973$ at the MDSC site is used in this formula (a value previously rejected as nonrepresentative of the entire plume), it can be seen that the increase in ω_o of +0.01 would result in a drop of optical depths of approximately 0.1, bringing the MDSC optical depth in Table 3 close enough to the AERONET measurement to be within satellite retrieval uncertainty.

[43] The estimated instrumental measurement uncertainty of absorption and scattering is 25% and 15%, respectively [*Taubman et al.*, 2004]. For most aerosols the absorption is much smaller than the scattering, so scattering uncertainties largely cancel when the ω_o ratio is calculated. For the assumed instrumental uncertainties in scattering and absorption the resulting uncertainty in ω_o is about 2% or 0.02 [*Reid et al.*, 1998a]. This matches the statistical sampling uncertainty, implying that instrumental variations in the measured properties may be as significant as spatial or temporal variations.

6.1.2. Surface Albedo

[44] The sensitivity of retrieved optical depth, τ, to the surface albedo depends on Sun-satellite geometry as well as the optical depth. To test this sensitivity a point was selected in the middle of the flight pattern to represent the typical geometry used in this study. For a fixed radiance measured by satellite, changes in the surface albedo are balanced by a contrary change in retrieved aerosol optical depth. Figure 10 shows "isorads" of constant radiance, in increments of 5 W/m². The changing slopes of the isorads indicate that the sensitivity of optical depth to surface reflectance decreases with optical depth. For a typical uncertainty in

Calculations of forcing using AERONET optical properties

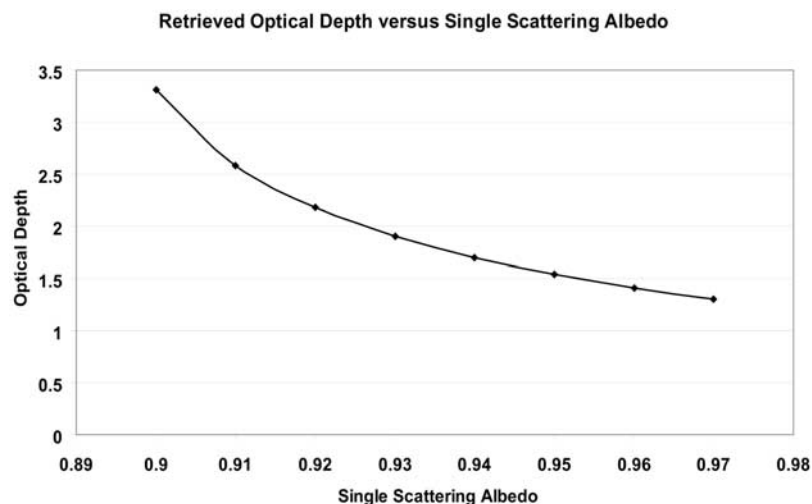TOA forcing

Surface forcing

Aerosol absorption

Calculations of forcing using in situ optical properties

Figure 8. Radiative forcing maps calculated from the optical depth retrievals and optical models. The top row is based on AERONET, and the bottom row is based on in situ data. For symbol definitions, see Figure 1. Gray areas are undefined data. The color scale ranges from 0 to 120 W/m^2 for TOA forcing and from 0 to 360 W/m^2 for the absorption and surface forcing. See color version of this figure at back of this issue.
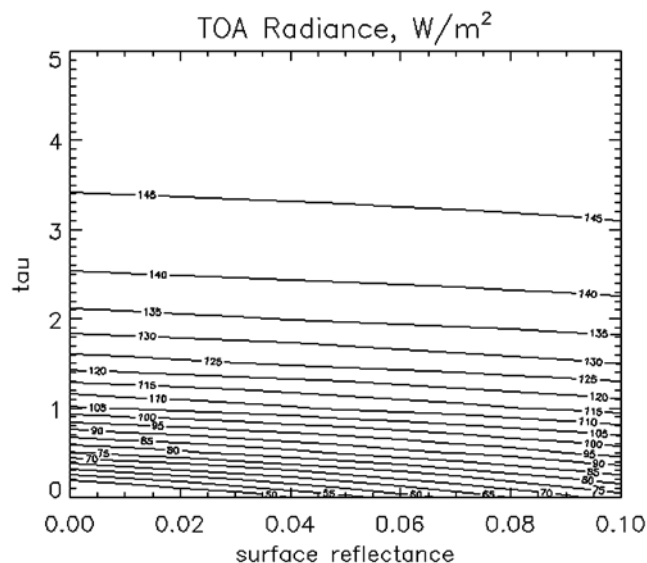
surface reflectance of ±.02 we can expect an uncertainty in optical depth of ±0.1 for optical depths close to 2, smaller for higher optical depths. This is about a 5% uncertainty for the optical depths measured at the AERONET sites.

6.1.3. Phase Function

[45] The phase functions were determined from the scattering Ångström exponents, which are assumed to be variable within one standard deviation of the average

Figure 9. Retrieved optical depth as a function of single scattering albedo for a sample TOA radiance.

Figure 10. Satellite observed radiance (contours) as a function of optical depth and surface reflectance. Radiance is in W/m^2/μm/steradian.

values. The sensitivity of retrieved optical depth of smoke to the perturbations in the Ångström exponents is shown in Table 5. Asymmetry factors are included as an indication of how the calculated optical properties are affected by these perturbations.

[46] The optical properties are affected more by the spread of the Ångström exponents than their actual magnitudes. For this case so long as the exponents are moved toward or away from each other by one standard deviation of their initial value, a change in optical depth of 15–20% is effected.

[47] The real part of the index of refraction also affects the derived phase functions. The bottom of Table 6 shows how the retrieval is very stable for 1.54 < n < 1.62, but produces large variations in optical depth when n becomes lower. Numerical tests of the AERONET algorithm [Dubovik et al., 2000] indicate that for a real refraction index of 1.45 and optical depths of 0.5, the accuracy is about ±.03, well within the stable range for this optical depth retrieval.

6.1.4. Boundary Layer Aerosol Thickness

[48] All the calculations above involving a two level model assume a constant boundary layer aerosol optical depth of 0.34 ± 0.1 in order to isolate the effect of smoke aerosol. While this value represents the average conditions of the background aerosol, the actual value is expected to vary across the region at the time of satellite overpass. The retrieved optical depth of the smoke layer must compensate for variations in the PBL layer, which is unrealistically held constant. The resulting uncertainty in smoke optical depth should thus be approximately equal to the 0.1 uncertainty of the PBL.

6.1.5. Total Uncertainty in Optical Depth

[49] Adding the above effects in quadrature results in a combined uncertainty of ±22% for the satellite retrieved optical depths close to 2 in the vicinity of the AERONET stations. This is sufficient to encompass the range of values calculated for the various optical models. From a satellite retrieval standpoint the optical properties as measured either

in situ or by AERONET are therefore equivalent given the current instrumental uncertainties for moderate optical depths.

6.2. Sensitivity in Determining Smoke Radiative Forcing

[50] Forcing calculations may be affected both by the retrieved optical depth at 550 nm and by the size distribution that dictates the ratios of optical depths across the spectrum. Changes in the imaginary index of refraction affect the retrieved optical depth without a significant effect on the size distributions calculated from scattering Ångström exponents. For the range of optical thicknesses retrieved in this study the calculated surface forcing is proportional to optical depth, so for an instrumental uncertainty in ω$_o$ of ±0.02, the uncertainties in smoke optical depth of 0.5% and 16% at the SURFRAD and ISIS sites, respectively, will yield the same uncertainties in surface forcing.

[51] The size distribution calculation, however, is affected by variations in both the assumed real index of refraction and the scattering Ångström exponents. Table 6 shows the effect of these possible variations at the ISIS site because the smoke loading at SURFRAD was too low to show appreciable effects.

[52] Sensitivity to the real part of the index of refraction was tested by shifting values throughout the spectrum equally, so that all comparisons can be referenced to the variation of n at 0.55 μm. As shown in Table 6 the value for the real index of refraction, n = 1.58, is within an area of stability for variations on the order of 0.04, with lower values leading to significantly higher retrieved forcings. Dropping the index of refraction as low as 1.54 at 0.55 μm (and hence even lower in the UV) without a significant change in radiative effects allows comparison to similar studies [Torres et al., 2002].

[53] Separation between scattering exponents has a larger effect than an equal shift in the value of both exponents: the closer together the exponents are, the broader the size distribution. When the size distribution is distorted the variation in TOA flux may not be related to the resulting changes in retrieved optical depth: even if the optical depth at 0.55 μm decreases, the broadband reflected flux may increase (Table 6). Once again, a broad distribution results in a more uniform forcing across the spectrum and an increased total forcing.

[54] Combining uncertainties in optical depth and size distribution leads to an estimated uncertainty in surface forcing of ~6% at the SURFRAD site (dominated by a fixed PBL layer), and ~19% at the ISIS site. The surface forcing calculated using the in situ measured optical prop-

Table 5. Retrieved Optical Depth of Smoke As a Function of the Scattering Phase Functions Derived From Scattering Ångström Exponents Measured in Situ[a]

	Angstrom Exponents	g	Tau GSFC
Average	$\alpha_{450/550} + 0$, $\alpha_{550/700} + 0$	0.662	1.90
High	$\alpha_{450/550} + SD$, $\alpha_{550/700} + SD$	0.656	1.87
Low	$\alpha_{450/550} - SD$, $\alpha_{550/700} - SD$	0.667	1.94
Tight	$\alpha_{450/550} + SD$, $\alpha_{550/700} - SD$	0.638	1.60
Wide	$\alpha_{450/550} - SD$, $\alpha_{550/700} + SD$	0.691	2.33

[a]Note that optical depth does not include PBL. SD, standard deviation.

Table 6. Effects of Variation of Scattering Ångström Exponents and Real Index of Refraction on Retrieved Radiative Forcing[a]

	Tau ISIS (Sterling, VA)	Surface Forcing, W/m^2	TOA Forcing, W/m^2
	Average Properties		
Total	**1.93**	**−297**	**−50**
PBL	**0.34**	**−64**	**−25**
	Ångström Exponent Variations		
Tight	1.66	−279	−54
Wide	2.28	−324	−44
Low	1.96	−299	−49
High	1.90	−295	−51
	Index of Refraction Variations		
n = 1.50	2.45	−345	−43
n = 1.54	1.97	−299	−49
n = 1.62	1.92	−298	−50

[a]Refer to Table 5 for explanation of the types of variations in the two exponents. The PBL aerosol layer was not varied.

erties falls within this range, while that calculated using the AERONET retrieved optical properties does not. The TOA flux may be compared across the entire region. Surface effects are highly variable across the spectrum and difficult to quantify. The possible variations due to aerosol alone contribute about 11% to the total uncertainty. As a result most of the TOA fluxes calculated for pixels in the thick part of the plume using the in situ data would fall within the range of the CERES measured TOA flux, while the AERONET based calculations would not.

7. Discussion

[55] It is seen that for this particular case, satellite retrievals of optical depth using in situ measurements as inputs are higher than those using AERONET retrievals as inputs. For most cases the discrepancy is within algorithm or instrument uncertainty, but for large optical depths the absorption becomes important and the optical depths diverge substantially. The accuracy of the calculated broadband forcings do not seem correlated to accuracies in optical depth. These discrepancies and inconsistencies are discussed below.

[56] Sensitivity studies demonstrate that the single scattering albedo is the major factor in satellite retrievals of optical depth; it is also the only optical parameter for which the difference between the AERONET and in situ data cannot be explained as the result of a column average. The differences between ω_o measured in situ and by AERONET may not be experimentally significant because the radii of error overlap (see also *Reid et al.* [1998b] or *Russell et al.* [2002], both of which compound statistical and instrumental uncertainty), but the effect on radiative calculations based on these measurements are substantial. In order for the in situ ω_o value of 0.93 to match the AERONET value of 0.964, either the absorption must be cut in half or the scattering must be doubled. This halving/doubling trend is also evident in comparison of the AERONET climatological average of 0.975 for the PBL as compared to the in situ measurement of 0.95 [*Dubovik et al.*, 2002; *Hartley et al.*, 2000]. The case of scattering measurements being largely responsible for the variation in ω_o may be discounted: scattering comprises more than 90% of the optical depth, and many field campaigns with

similar instrumentation have verified agreement in optical depth between aircraft in situ measurements and Sun photometers using retrievals similar to that currently used by AERONET [*Hegg et al.*, 1997; *Remer et al.*, 1997; *Russell et al.*, 1999a, 1999b; *Ross et al.*, 1998; *Fiebig et al.*, 2002; *Kato et al.*, 2000; *Haywood et al.*, 2003; *Magi et al.*, 2003]. Given the small absorption/scattering ratio, accuracy in scattering almost certainly falls within the maximum relative uncertainty in optical depth found in these comparisons.

[57] Many of the column closure studies listed above claim success when measurements of optical depth agree within twenty percent and ω_o to within a few percent. With absorption typically a small fraction of scattering, the use of optical depth as an evaluation of column closure places weak constraints on the absorption, which could vary by a factor of two while only affecting the optical depth and ω_o by a few percent. For use in satellite retrievals of thick plumes a higher confidence in the measurement of ω_o is required. It should be noted that the uncertainty for the MODIS aerosol retrieval is quoted as $\pm(0.2\tau + .05)$, which is 25% or less for optical depths above one. This study suggests that if the typical uncertainty in single scattering albedo is $\pm(.02$ to $.03)$ the uncertainty in optical depth may exceed that quoted for the MODIS retrieval once the optical depth becomes as large as 1.5 (see Figure 5 and equation (1)). However, given the differences between the MODIS algorithm and the one used in this paper, such a statement cannot be viewed as definitive (a description of the MODIS algorithm may be found in the work of *Kaufman and Tanre* [1998]).

[58] Before turning to the absorption measurements themselves to explain discrepancies in single scattering albedo measurements, another option must be addressed. Perhaps the assumption of fixed inputs may be relaxed to allow variations in optical properties. Past studies have shown that the optical properties of smoke change with optical depth, even within the same plume [*Dubovik et al.*, 2002; *Wong and Li*, 2002; *Remer et al.*, 1998]. For smoke the trend as the optical depth increases is for the single scattering albedo to increase while the asymmetry parameter decreases [*Wong and Li*, 2002]. These two parameters reinforce the effects of each other as seen by a satellite at TOA, resulting in a decrease in retrieved optical depth. Unfortunately the relationship between optical depth and optical properties as

derived by *Wong and Li* [2002] is not a firm one, and is likely to vary with aerosol type and ambient conditions. For this particular plume there is not yet sufficient information to draw relationships between measurements in different locations such as the AERONET sites and aircraft spirals. Further analysis of the aircraft data is underway to determine the extent of changes in optical properties related to particle number density.

[59] In situ absorption measurements remain as the primary factor in disagreements between optical depth retrievals via satellite and AERONET, despite the fact that the PSAP is highly regarded as an instrument for the measurement of in situ absorption [*Reid et al.*, 1999a]. The measurements presented here are not likely to be outliers due to instrument operation: several in situ measurements of boundary layer aerosols in this area by systems equivalent to the one used in this paper indicate the same value of ω_o = 0.95 as seen in this paper [*Hartley et al.*, 2000; *Hegg et al.*, 1997], and since the absorption measurements were performed at ambient temperature no humidity corrections were required [*Taubman et al.*, 2004].

[60] The *Bond et al.* [1999] calibration used for this and most other papers that use the PSAP is based on a single standard aerosol of absorptive hydrocarbon. Different aerosols may be expected to respond differently to heating effects or interaction with the filter. The Bond correction equations account for scattering effects based on the aerosol used for calibration (n = 1.67 at a wavelength of 0.55 microns). Since scattering is typically so much larger than absorption, this is not a negligible correction. The difference between the index of refraction of different aerosols and filter will affect scattering. The shape of the liquid component of many aerosols may also be distorted by contact with the filter matrix. The calibration used a solid aerosol: aged smoke aerosol is assumed to be a solid core with a liquid sheath [*Bundke et al.*, 2002]. LACE-98 recalibrated their PSAP following the Bond procedure but with a different standard aerosol [*Bundke et al.*, 2002; *Bond et al.*, 1999]; the agreement between their Sun photometers and PSAP may have been the result.

[61] Broadband forcing at the surface is mainly the result of scattering of short-wave radiation. Extrapolation of the scattering across the spectrum using the in situ measurements resulted in integrated flux values much closer to those measured by SURFRAD and CERES than did forcings using the AERONET optical properties. Since the forcing is an extrapolated calculation based on a retrieved optical depth, this represents a contradiction to the previous result that the satellite retrieved optical depth based on AERONET-derived optical properties was closer to observations than in situ based retrievals. Though the AERONET retrievals should represent a consistent set of optical properties it is possible that the assumption of an equivalent monomodal size distribution instead of the indicated bimodal distribution is responsible for these differences. There is no simple algorithm to find a monomodal size distribution that is optically equivalent to a given bimodal distribution [*Tanre et al.*, 1996]. Given the multiple measurements, assumptions, and calculational steps necessary for the forcing calculations it is possible that a systematic bias may favor the forcing calculations for higher optical depths. The CERES flux retrievals are based on assumed

anisotropies in the radiation field stemming from broad categories of surface type, and the resulting uncertainties are difficult to quantify. A few measurements are not sufficient to clearly establish a pattern, other than to state that comparisons between optical depth retrievals at a single wavelength may not imply similar results for broadband calculations based on the commonly available data gathering techniques used for this study.

8. Conclusions

[62] Optical depth for a thick smoke plume was calculated from satellite reflectances combined with two sets of aerosol optical parameters: a complete set of AERONET retrieved optical properties and a complete set of optical properties derived from in situ measurements by aircraft. Two blended models used mixtures of AERONET and in situ measured optical properties in the smoke layer. The optical depth using AERONET ω_o with in situ–derived scattering phase functions were 2% to 16% lower than the direct AERONET observations of optical depth, while retrievals using in situ measured absorption produced optical depths that were 22% to 43% larger than the observations. Algorithm uncertainties increased with optical depth, although for the observed optical depths of $\sim$2 the total uncertainty for most retrievals overlapped those of the other models.

[63] The larger optical depths retrieved using in situ–derived optical properties is due to the lower reflectivity of the assumed aerosol. This low reflection can be traced mainly to the absorption measurement, which is twice as large as that inferred from AERONET. Multiple scattering enhances the effects of variations in absorptivity [*Bohren*, 1987].

[64] Broadband fluxes calculated from the in situ optical properties matched surface and TOA observations better (21% error) than those calculated from AERONET retrieved optical properties (33% error). In this calculation satellite retrieved optical depth was extrapolated across the solar spectrum based on the measured size distributions. This apparent inconsistency between which optical depth retrievals best matched the AERONET observations and which forcing calculations best matched the surface and TOA observations may be due to compounding a larger set of measurements and assumptions into calculation of the forcing retrievals.

[65] Achieving accuracy and consistency between different types of absorption measurement presents a significant challenge to the aerosol community. Satellites present the best way to track aerosol plumes, but unless the retrieval algorithms have accurate single scattering albedos, optical depth measurements (and hence forcing calculations) cannot be done with reasonable accuracy. Forcing calculations require a larger number of measurements (or extrapolation) and hence are even more susceptible to accuracy in optical properties. This situation is demonstrated by this study in which the differences between the optical properties measured in situ and by AERONET were within instrumental uncertainty but the radiative calculations based upon these measurements varied widely. The sensitivity studies in this paper indicate that the uncertainty in optical depth is roughly proportional to the optical depth itself raised to

the 5/2 power, so since most aerosol loading is rather low, this problem has attracted little past attention.

References

Ackerman, A., O. B. Toon, and P. V. Hobbs (1995), Numerical modeling of ship tracks produced by injection of cloud condensation nuclei into marine stratiform clouds, *J. Geophys. Res.*, *100*(D4), 7121–7133.

Ackerman, A., O. B. Toon, D. E. Stevens, A. J. Heymsfield, V. Ramanathan, and E. J. Welton (2000), Reduction of tropical cloudiness by soot, *Science*, *288*, 1042–1047.

Bergstrom, R., P. Russell, and P. Hignett (2002), Wavelength dependence of the absorption of black carbon particles: Predictions and results from the TARFOX experiment and implications for the aerosol single scattering albedo, *J. Atmos. Sci.*, *59*, 567–577.

Bohren, C. (1987), Multiple scattering of light and some of its observable consequences, *Am. J. Phys.*, *55*, 524–533.

Bohren, C., and D. Huffman (1983), *Absorption and Scattering of Light by Small Particles*, John Wiley, Hoboken, N. J.

Bond, T. C., T. L. Anderson, and D. Campbell (1999), Calibration and intercomparison of filter-based measurements of visible light absorption by aerosols, *Aerosol Sci. Technol.*, *30*, 582–600.

Bundke, U., G. Hänel, H. Horvath, W. Kaller, S. Seidl, H. Wex, A. Wiedensohler, M. Wiegner, and V. Freudenthaler (2002), Aerosol optical properties during the Lindenberg Aerosol Characterization Experiment (LACE 98), *J. Geophys. Res.*, *107*(D21), 8123, doi:10.1029/2000JD000188.

Chang, F., Z. Li, and S. Ackerman (2000), Examining relationships between cloud and radiation quantities derived from satellite observations and model calculations, *J. Clim.*, *13*, 3842–3859.

Chang, H., and T. Charalampopoulos (1990), Determination of the wavelength dependence of refractive indices of soot, *Proc. R. Soc. London*, *430*, 577–591.

Conny, J. M., and J. F. Slater (2002), Black carbon and organic carbon in aerosol particles from crown fires in the Canadian boreal forest, *J. Geophys. Res.*, *107*(D11), 4116, doi:10.1029/2001JD001528.

Dubovik, O., A. Smirnov, B. N. Holben, M. D. King, Y. J. Kaufman, T. F. Eck, and I. Slutsker (2000), Accuracy assessments of aerosol optical properties retrieved from Aerosol Robotic Network (AERONET) Sun and sky radiance measurements, *J. Geophys. Res.*, *105*, 9791–9806.

Dubovik, O., B. Holben, T. F. Eck, A. Smirnov, Y. J. Kaufman, M. D. King, D. Tanre, and I. Slutsker (2002), Variability of absorption and optical properties of key aerosol types observed in worldwide locations, *J. Atmos. Sci.*, *59*, 590–608.

Eck, T. F., B. N. Holben, J. S. Reid, N. T. O'Neill, J. S. Schafer, O. Dubovik, A. Smirnov, M. A. Yamasoe, and P. Artaxo (2003), High aerosol optical depth biomass burning events: A comparison of optical properties for different source regions, *Geophys. Res. Lett.*, *30*(20), 2035, doi:10.1029/2003GL017861.

Fiebig, M., A. Petzold, U. Wandinger, M. Wendisch, C. Kiemle, A. Stifter, M. Ebert, T. Rother, and U. Leiterer (2002), Optical closure for an aerosol column: Method, accuracy, and inferable properties applied to a biomass-burning aerosol and its radiative forcing, *J. Geophys. Res.*, *107*(D21), 8130, doi:10.1029/2000JD000192. (Correction, *J. Geophys. Res.*, *108*(D6), 8133, doi:10.1029/2003JD001605, 2003.)

Green, R., and J. Robbins (1997), ERBE-like inversion to instantaneous TOA flux: Algorithm theoretical basis document, *Release 2.2*, 37 pp., NASA Langley Res. Cent., Hampton, Va.

Hartley, S., P. Hobbs, J. Ross, P. Russell, and J. Livingston (2000), Properties of aerosols aloft relevant to direct radiative forcing off the mid-Atlantic coast of the United States, *J. Geophys. Res.*, *105*, 9859–9885.

Haywood, J. M., S. R. Osborne, P. N. Francis, A. Keil, P. Formenti, M. O. Andreae, and P. H. Kaye (2003), The mean physical and optical properties of regional haze dominated by biomass burning aerosol measured from the C-130 aircraft during SAFARI 2000, *J. Geophys. Res.*, *108*(D13), 8473, doi:10.1029/2002JD002226.

Hegg, D., J. Livingston, P. Hobbs, T. Novakov, and P. Russell (1997), Chemical apportionment of aerosol column optical depth off the mid-Atlantic coast of the United States, *J. Geophys. Res.*, *102*, 25,293–25,303.

Hobbs, P. V., J. S. Reid, R. A. Kotchenruther, R. J. Ferek, and R. Weiss (1997), Direct radiative forcing by smoke from biomass burning, *Science*, *275*, 1777–1778.

Holben, B., et al. (1998), AERONET—A federated instrument network and data archive for aerosol characterization, *Remote Sens. Environ.*, *66*, 1–16.

Kato, S., et al. (2000), A comparison of the aerosol thickness derived from ground-based and airborne measurements, *J. Geophys. Res.*, *105*, 14,701–14,717.

Kaufman, Y. J., and R. Fraser (1997), The effect of smoke particles on clouds and climate forcing, *Science*, *277*, 1636–1639.

Kaufman, Y. J., and D. Tanre (1998), Algorithm for remote sensing of tropospheric aerosol from MODIS: Algorithm theoretical basis document, 85 pp., NASA Goddard Space Flight Cent., Greenbelt, Md.

Kaufman, Y. J., R. Fraser, and R. Ferrare (1990a), Satellite measurements of large-scale pollution: Methods, *J. Geophys. Res.*, *95*, 9895–9909.

Kaufman, Y. J., C. J. Tucker, and I. Fung (1990b), Remote sensing of biomass burning in the tropics, *J. Geophys. Res.*, *95*, 9927–9939.

Kaufman, Y. J., et al. (1998), Smoke, Clouds, and Radiation-Brazil (SCAR-B) Experiment, *J. Geophys. Res.*, *103*(D24), 31,783–31,808.

Kaufman, Y. J., D. Tanre, and O. Bouchier (2002), A satellite view of aerosols in the climate system, *Nature*, *419*, 215–223.

King, M. D., Y. J. Kaufman, D. Tanre, and T. Nakajima (1999), Remote sensing of tropospheric aerosols from space: Past, present, and future, *Bull. Am. Meteorol. Soc.*, *80*, 2229–2259.

Kreidenweis, S., L. Remer, R. Bruintjes, and O. Dubovik (2001), Smoke aerosol from biomass burning in Mexico: Hygroscopic smoke optical model, *J. Geophys. Res.*, *106*, 4831–4844.

Li, Z. (1998), Influence of absorbing aerosols on the inference of solar surface radiation budget and cloud absorption, *J. Clim.*, *11*, 5–17.

Li, Z., and L. Kou (1998), Atmospheric direct radiative forcing by smoke aerosols determined from satellite and surface measurements, *Tellus, Ser. B*, *50*, 543–554.

Magi, B. I., P. V. Hobbs, B. Schmid, and J. Redemann (2003), Vertical profiles of light scattering, light absorption, and single scattering albedo during the dry, biomass burning season in southern Africa and comparisons of in situ and remote sensing measurements of aerosol optical depths, *J. Geophys. Res.*, *108*(D13), 8504, doi:10.1029/2002JD002361.

Miller, J., and T. O'Neill (1997), Multilatitude airborne observations of insolation effects of forest fire smoke aerosols at BOREAS: Estimates of aerosol optical properties, *J. Geophys. Res.*, *102*, 29,729–29,736.

Mishchenko, M. I., L. D. Travis, and A. A. Lacis (2002), *Scattering, Absorption, and Emission of Light by Small Particles*, Cambridge Univ. Press, New York.

Novakov, T., D. Hegg, and P. Hobbs (1997), Airborne measurements of carbonaceous aerosols on the east coast of the United States, *J. Geophys. Res.*, *102*, 30,023–30,030.

Penner, J. E., R. E. Dickinson, and C. A. O'Neill (1992), Effects of aerosol from biomass burning on the global radiation budget, *Science*, *256*, 1432–1434.

Ramanathan, V., P. J. Crutzen, J. T. Kiehl, and D. Rosenfeld (2001a), Aerosols, climate, and the hydrological cycle, *Science*, *294*, 2119–2123.

Ramanathan, V., et al. (2001b), Indian Ocean Experiment: An integrated analysis of the climate forcing and effects of the great Indo-Asian haze, *J. Geophys. Res.*, *106*, 28,371–28,398.

Reid, J. S., P. Hobbs, C. Liousse, J. Martins, R. Weiss, and T. Eck (1998a), Comparisons of techniques for measuring shortwave absorption and black carbon content of aerosols from biomass burning in Brazil, *J. Geophys. Res.*, *103*, 32,031–32,040.

Reid, J. S., P. V. Hobbs, R. J. Ferek, D. R. Blake, J. V. Martins, J. V. Dunlap, and C. Liousse (1998b), Physical, chemical, and optical properties of regional hazes dominated by smoke in Brazil, *J. Geophys. Res.*, *103*, 32,059–32,080.

Reid, J. S., T. F. Eck, S. A. Christopher, P. V. Hobbs, and B. Holben (1999), Use of the Ångstrom exponent to estimate the variability of optical and physical properties of aging smoke particles in Brazil, *J. Geophys. Res.*, *104*, 27,473–27,489.

Remer, L. A., S. Gasso, D. A. Hegg, Y. J. Kaufman, and B. N. Holben (1997), Urban/industrial aerosol: Ground based Sun/sky radiometer and airborne in situ measurements, *J. Geophys. Res.*, *102*, 16,849–16,859.

Remer, L. A., Y. J. Kaufman, B. N. Holben, A. M. Thompson, and D. McNamara (1998), Biomass burning aerosol size distribution and modeled optical properties, *J. Geophys. Res.*, *103*, 31,879–31,891.

Ricchiazzi, P., S. Yang, D. Gautier, and D. Sowle (1998), SBDART: A research and teaching software tool for plane-parallel radiative transfer in the Earth's atmosphere, *Bull. Am. Meteorol. Soc.*, *79*, 2101–2114.

Rosenfeld, D. (1999), TRMM observed first direct evidence of smoke from forest fires inhibiting rainfall, *Geophys. Res. Lett.*, *26*, 3105–3108.

Ross, J. L., P. Hobbs, and B. Holben (1998), Radiative characteristics of regional hazes dominated by smoke from biomass burning in Brazil: Closure tests and direct radiative forcing, *J. Geophys. Res.*, *103*, 31,925–31,941.

Russell, P. B., J. Livingston, P. Hignett, S. Kinne, J. Wong, A. Chien, R. Bergstrom, P. Durkee, and P. Hobbs (1999a), Aerosol-induced radiative flux changes off the United States mid-Atlantic coast: Comparison of values calculated from Sun photometer and in situ data with those measured by airborne pyranometer, *J. Geophys. Res.*, *104*, 2289–2307.

Russell, P. B., P. Hobbs, and L. Stowe (1999b), Aerosol properties and radiative affects in the United States east coast haze plume: An overview of the Tropospheric Aerosol Radiative Forcing Observational Experiment (TARFOX), *J. Geophys. Res.*, *104*, 2213–2222.

Russell, P. B., et al. (2002), Comparison of aerosol single scattering albedos derived by diverse techniques in two North Atlantic experiments, *J. Atmos. Sci.*, *59*, 609–619.

Tanre, D., M. Herman, and Y. Kaufman (1996), Information on aerosol size distribution contained in solar reflected spectral radiances, *J. Geophys. Res.*, *101*, 19,043–19,060.

Taubman, B. F., L. T. Marufu, B. L. Vant-Hull, C. A. Piety, B. G. Doddridge, R. R. Dickerson, and Z. Li (2004), Smoke over haze: Aircraft observations of chemical and optical properties and the effects on heating rates and stability, *J. Geophys. Res.*, *109*, D02206, doi:10.1029/2003JD003898.

Torres, O., P. K. Bhartia, J. R. Herman, A. Sinyuk, P. Ginoux, and B. Holben (2002), A long-term record of aerosol optical depth from TOMS observations and comparison to AERONET measurements, *J. Atmos. Sci.*, *59*, 398–413.

Vermote, E., and A. Vermeulen (1999), Atmospheric correction algorithm, spectral reflectances (MOD09): Algorithm theoretical basis document, version 4.0, 103 pp., NASA Goddard Space Flight Cent., Greenbelt, Md.

Wang, J., S. A. Christopher, F. Brechtel, J. Kim, B. Schmid, J. Redemann, P. B. Russell, P. Quinn, and B. N. Holben (2003), Geostationary satellite retrievals of aerosol optical thickness during ACE-Asia, *J. Geophys. Res.*, *108*(D23), 8657, doi:10.1029/2003JD003580.

Wong, J., and Z. Li (2002), Retrieval of optical depth for heavy smoke aerosol plumes: Uncertainties and sensitivities to the optical properties, *J. Atmos. Sci.*, *59*, 250–261.
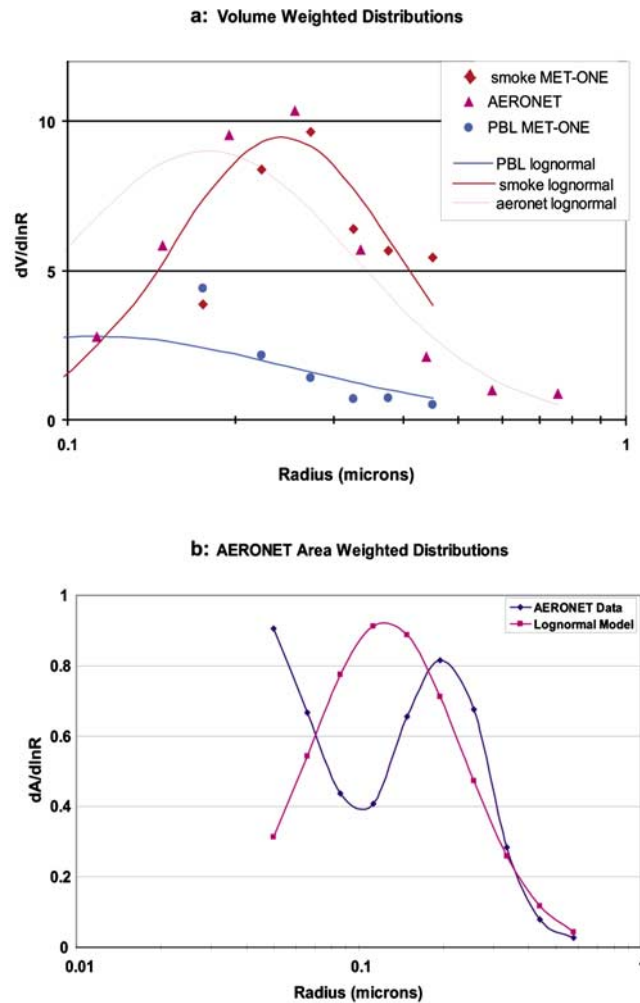
————————————

F.-L. Chang and Z. Li, Earth Systems Science Interdisciplinary Center, College Park, MD 20742, USA.

R. R. Dickerson and B. F. Taubman, Department of Chemistry, University of Maryland, College Park, MD 20742, USA.
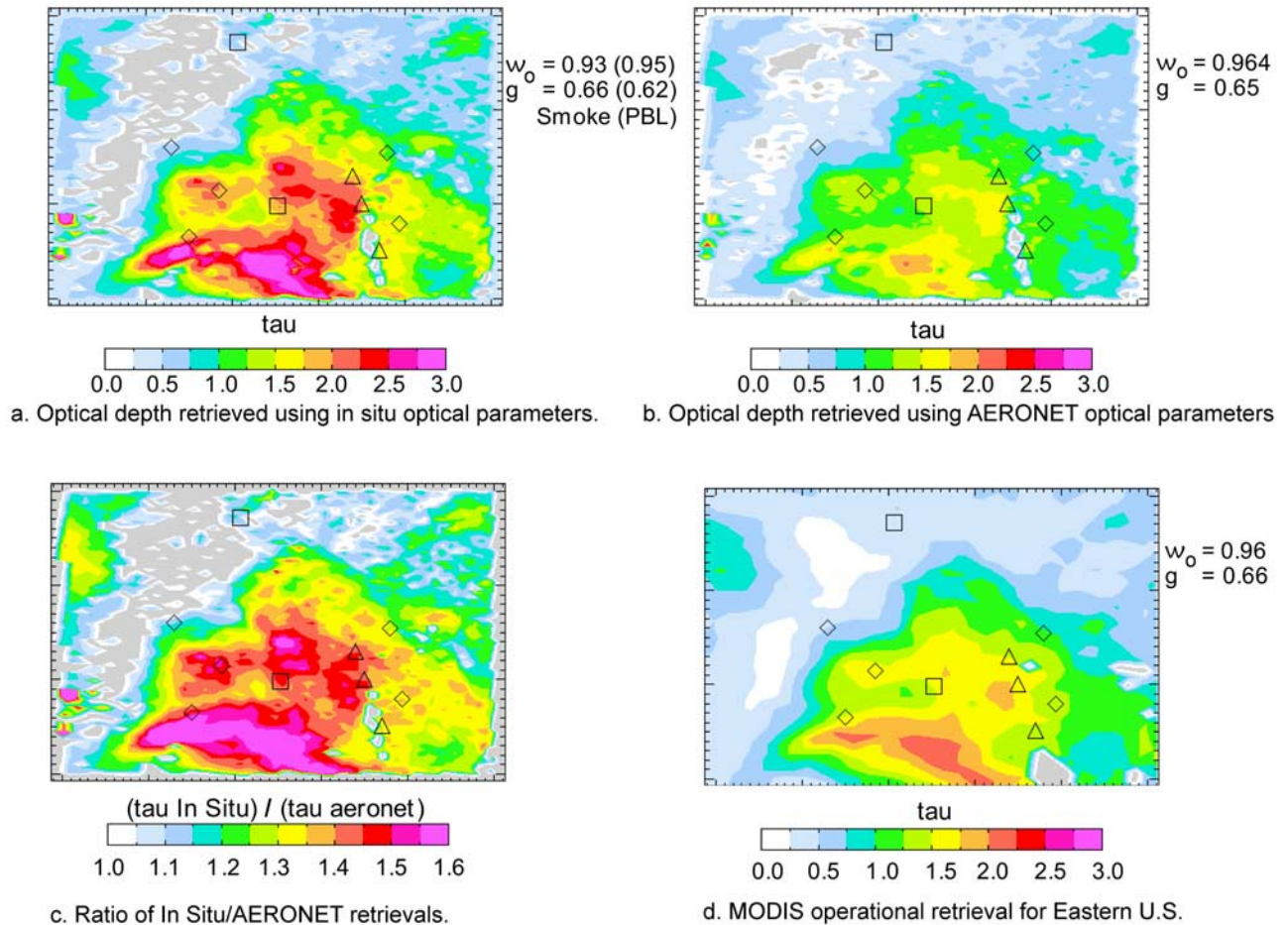
B. G. Doddridge, L. Marufu, and B. Vant-Hull, Department of Meteorology, University of Maryland, College Park, MD 20742, USA. (brianvh@atmos.umd.edu)

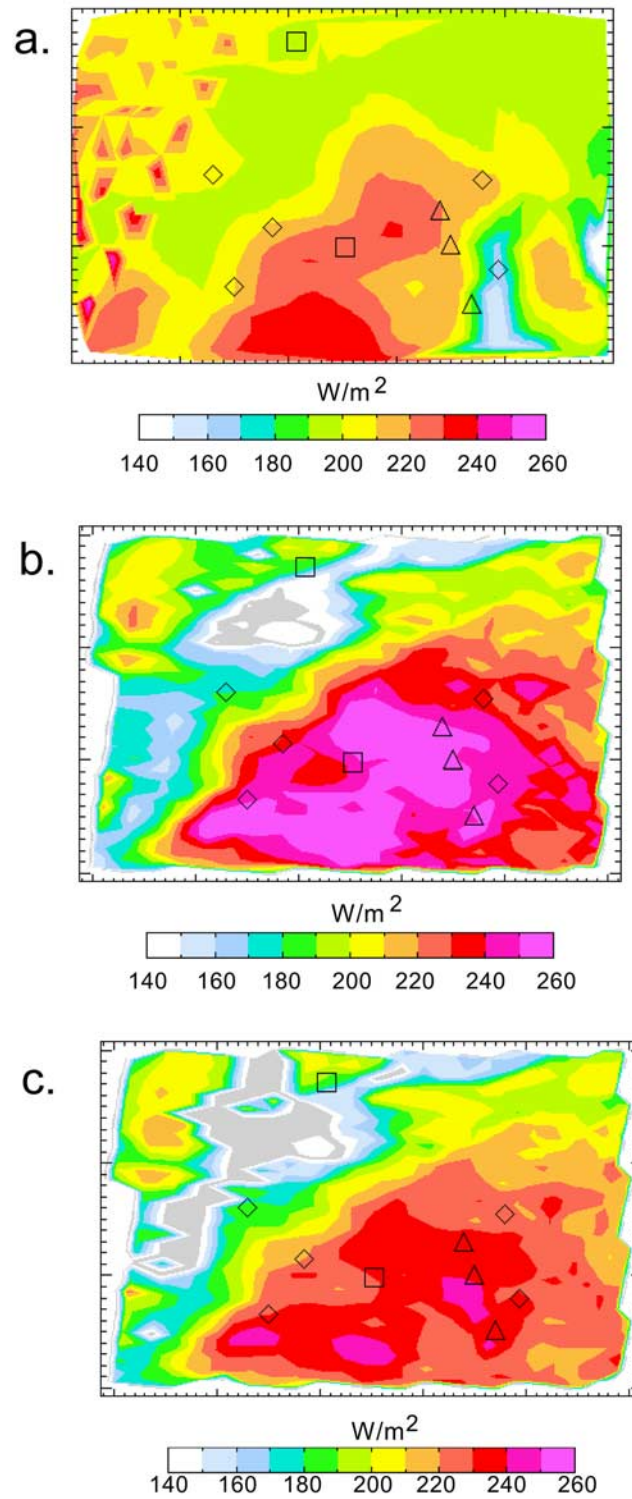R. Levy, Goddard Space Flight Center, Greenbelt, MD 20771, USA.

Figure 2. (a) Population per cubic centimeter: Met One smoke data points (diamonds), Met One PBL aerosol data points (circles), and AERONET retrievals (triangles). The solid lines are lognormal fits to scattering Angstrom exponents from in situ data. The dotted line is based on statistics from the AERONET retrieval. The amplitude of each lognormal curve is adjusted to best fit for all points. (b) Area weighted distribution for the AERONET retrieval (blue) and the lognormal curve based on statistics from the retrieval. Vertical units are arbitrary.
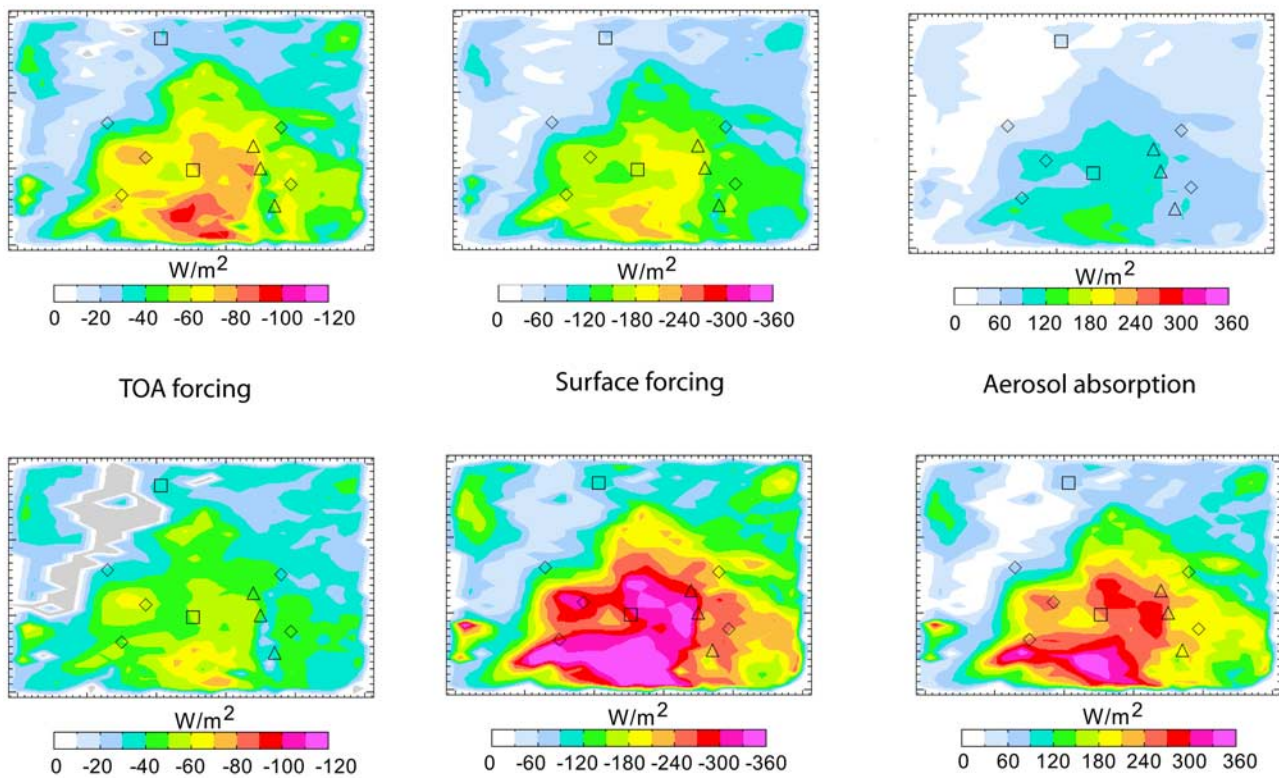
Figure 5. Comparison of optical depth retrievals via satellite. For symbol definition, see Figure 1. The color scale ranges from 1 to 3. (a) Optical depth retrieved using in situ optical parameters. (b) Optical depth retrieved using AERONET optical parameters. (c) Ratio of in situ/AERONET retrievals. (d) MODIS operational retrieval for the eastern United States.

Figure 7. Comparisons of flux measurements to calculations from the two primary optical models. For symbol definitions, see Figure 1. The gray areas are undefined data. (a) TOA flux retrieved by CERES. (b) TOA flux calculated from the AERONET model. (c) TOA flux calculated from the in situ model.

Figure 8. Radiative forcing maps calculated from the optical depth retrievals and optical models. The top row is based on AERONET, and the bottom row is based on in situ data. For symbol definitions, see Figure 1. Gray areas are undefined data. The color scale ranges from 0 to 120 W/m^2 for TOA forcing and from 0 to 360 W/m^2 for the absorption and surface forcing.